

Temporal impulse response of the Talbot interferometer

Hans Knuppertz^{a,*}, Jürgen Jahns^a, Rüdiger Grunwald^b

^a *Optische Nachrichtentechnik, FernUniversität Hagen, Universitätsstraße 27, 58084 Hagen, Germany*

^b *Max Born Institute for Nonlinear Optics and Short Pulse Spectroscopy, Max-Born-Straße 2A, 12489 Berlin, Germany*

Received 4 December 2006; received in revised form 27 April 2007; accepted 4 May 2007

Abstract

The Talbot interferometer has been shown earlier to act as an optical tapped delay-line in the time domain. The interferometer is based on the self-imaging effect. It consists of two gratings separated by a multiple of the self-imaging distance. Here, we determine its temporal behaviour experimentally. First, the impulse response is measured directly in the time domain by means of femtosecond pulse technology and second, by spectroscopy we measure its power spectrum. Results confirm earlier theoretical considerations.

© 2007 Elsevier B.V. All rights reserved.

PACS: 42.30.-d; 42.79.-e; 42.79.Dj; 42.79.Hp

Keywords: Talbot interferometer; Temporal impulse response; Optical tapped delay-line

1. Introduction

The Talbot self-imaging phenomenon has been known since 1836 [1] and investigated by many authors. Talbot self-imaging occurs, for example, when a grating G_1 of period p is illuminated by a monochromatic plane wave of wavelength λ . Then, at multiples of the “Talbot distance” $z_T = 2p^2/\lambda$ an interference pattern occurs that is identical to the one immediately behind the input object (disregarding experimental deficiencies). This effect has been used, for example, for phase interferometry [2] where a second grating G_2 is used to probe the wavefield generated by G_1 as shown in Fig. 1a.

Most of the earlier work related to Talbot self-imaging was performed by considering its *spatial* aspects. Recently, however, it was suggested to use the Talbot interferometer as a *temporal* device [3] for applications such as filtering, correlation and multiplexing. The basic effect used are different path lengths of diffraction orders in a dispersion-free medium. The temporal application of the spatial Talbot

effect must not be confused with the temporal Talbot effect [4] where the spectral lines of a frequency comb are delayed in a dispersive medium, usually a fiber. After a certain distance, the individual delays create a situation where all discrete frequencies of the comb are again in phase. This situation occurs at multiples of the characteristic distance. This repetition of equal phases is analog to the spatial Talbot effect. While this temporal Talbot effect uses different temporal frequencies, the spatial Talbot effect uses different discrete spatial frequencies.

The spatial Talbot interferometer can be described as follows. If G_1 and G_2 are implemented lithographically as phase gratings and, in particular, for $G_2 = G_1^*$ the diffraction orders generated by G_1 can be recombined efficiently by G_2 in a single output beam by coherent coupling. Thus, the zeroth order beam behind G_2 is the result of the combination of the $+n$ th order diffraction at the first grating and the $-n$ th order at the second grating. The separation of the gratings by a multiple of the Talbot distance ensures that the various diffraction orders are again in phase and thus leads to a high efficiency of the interferometer.

Here, we consider the use of the spatial Talbot interferometer for the processing of ultrashort optical pulses. The time delays are caused by the different path lengths that the

* Corresponding author. Tel.: +49 2331 987 1128; fax: +49 2331 987 352.

E-mail address: hans.knuppertz@fernuni-hagen.de (H. Knuppertz).

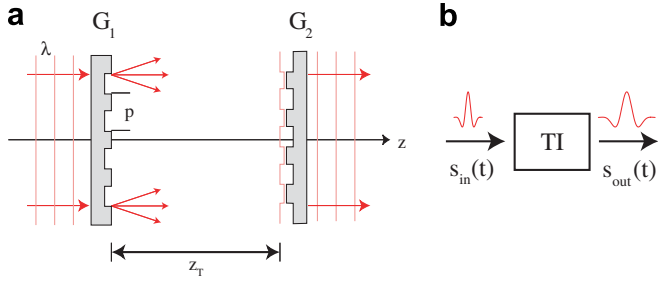


Fig. 1. The Talbot interferometer (a) consists of two gratings separated by a finite distance, often chosen to be a multiple of the self-imaging distance, z_T . If phase gratings are used, the diffraction orders generated by the first grating can be recombined by the second (see explanations in the text). (b) The Talbot interferometer can be used as a temporal device: the input signal is denoted as $s_{in}(t)$, the output signal as $s_{out}(t)$.

diffraction orders travel between the two gratings. When a short optical pulse passes through the interferometer, one can therefore expect to obtain a limited chain of pulses at the output. In terms of system theory, the Talbot interferometer then is to classify as finite impulse response (FIR) filter. Another optical filter of this type is the arrayed waveguide grating (AWG). Examples for the class of infinite impulse response filters are all kinds of resonators, e.g., ring resonators or chamber resonators (Fabry–Perot, etc.).

In this article, we demonstrate the operation of the Talbot interferometer in the time domain and discuss the limitations of this device. The experiments in the temporal domain were performed with fs-pulses to determine the impulse response. In addition, the spectral behaviour in the temporal frequency domain was investigated by using a tunable laser. This measurement yields the power spectrum transmission which is Fourier-related to the autocorrelation of the temporal impulse response. Within the practical limits of the experiments our results confirm the theoretical predictions.

This article is organized in the following way: in Section 2, we will review the temporal aspects of the Talbot interferometer. Section 3 deals with the modeling of the experiment. In Section 4, the measurement of the impulse response is described and results will be discussed. Section 5 features the measurement in the spectral domain to determine the power spectrum of the interferometer. In the final Section 6, we discuss the findings and present an outlook.

2. Talbot interferometer as a temporal device

In this section, we briefly review earlier results [3,5] about the Talbot interferometer as a temporal device. We consider the Talbot interferometer as shown in Fig. 1 consisting of gratings G_1 and G_2 . We assume a collimated quasi-monochromatic illumination of wavelength λ . (The case of polychromatic illumination will be discussed later). Grating G_1 and its complementary counterpart $G_2 = G_1^*$ are separated by a multiple of the Talbot distance, i.e., $\Delta z = Mz_T$ ($M = 1, 2, 3, \dots$). G_2 compensates the wavefront generated by G_1 and ideally, a single collimated beam

will propagate behind G_2 . This can be detected conveniently by a point detector in the rear focal plane of a lens.

To understand the temporal behavior of the Talbot interferometer we consider Fig. 2. Since the wavefield between the two gratings consists of the diffraction orders traveling under different angles, modal dispersion occurs. The propagation time for each diffraction order can easily be calculated. For the n th diffraction order with the tilt angle α_n we obtain the propagation time [5]

$$t_n = \frac{\Delta z}{c} \frac{1}{\sqrt{1 - \sin^2(\alpha_n)}} = \frac{\Delta z}{c} \frac{1}{\sqrt{1 - \frac{n^2 \lambda^2}{p^2}}}. \quad (1)$$

By simple calculus we obtain for the delay τ_n between the n th and the zeroth order

$$\tau_n = t_n - t_0 \approx n^2 \frac{\Delta z}{c} \frac{\lambda^2}{2p^2} = n^2 \frac{\lambda \cdot M}{c} = n^2 \tau_1, \quad n = 1, 2, 3, \dots \quad (2)$$

Here, we assumed the paraxial approximation. Note the quadratic increase of the time delays. The Talbot interferometer acts as a discrete linear time-invariant filter and can be represented by the mathematical structure shown in Fig. 3. The input signal $s_{in}(t)$ is split up into N branches, the diffraction orders. The n th branch is delayed by τ_n and weighted by a coefficient a_n . Finally, the different branches are recombined. This step is accomplished in the setup by grating G_2 . The diagram in Fig. 3 is known as a tapped delay-line (also as “finite impulse response filter”). However, whereas, usually a tapped delay-line generates a uniform sequence of delays, the Talbot interferometer generates time delays which increase quadratically with the index of the diffraction order.

For quasi-monochromatic illumination, i.e., pulse durations longer than typically $100\lambda/c$ the impulse response of the Talbot interferometer can be written as:

$$h(t) = \sum_{n=0}^N a_n \delta(t - \tau_n) = \sum_{n=0}^N a_n \delta(t - n^2 \tau_1). \quad (3)$$

The action of the Talbot interferometer on an input signal $s_{in}(t)$ is described mathematically by a convolution:

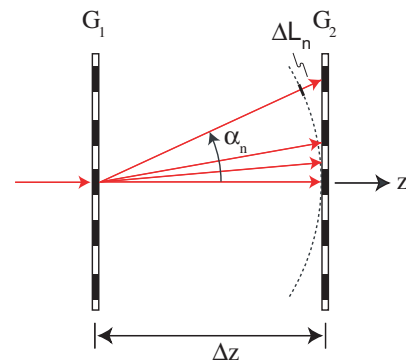


Fig. 2. The optical path length difference between the n th and the zeroth diffraction order is ΔL_n . It leads to a temporal delay according to Eq. (2).

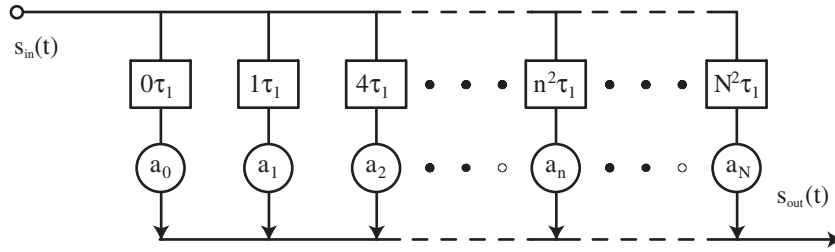


Fig. 3. Computational structure of a tapped-delay line, shown here for the specific parameters of the Talbot interferometer, i.e., a quadratic dependency of the time delays according to Eq. (2).

$$s_{out}(t) = s_{in}(t) * h(t). \tag{4}$$

To investigate the temporal behavior of the Talbot interferometer measurements can be carried out either in the temporal domain or in the frequency (i.e., spectral) domain. For describing the performance in the frequency domain, we use the transfer function which is given as the Fourier transform of the impulse response. With f the temporal frequency the Fourier transformation of Eq. (3) yields:

$$H(f) = \sum_{n=0}^N a_n \exp(2i\pi n^2 \tau_1 f). \tag{5}$$

For the measurement, it is actually the power spectrum $|H(f)|^2$ that can be recorded by a spectrometer. The coefficients a_n of the tapped-delay line are determined by the amplitudes of the diffraction orders. If b_n are the coefficients generated by the first grating G_1 and b_n^* are the coefficients for the complementary grating G_2 , then the filter coefficients are $a_n = |b_n|^2$. If we describe the amplitude transmission function of G_1 by $g(x)$ and assume that it is a phase-only grating, i.e., $g(x) = \exp[i\varphi(x)]$, b_n can be calculated using the integral

$$b_n = b_n(f) = \frac{1}{p} \int_{-p/2}^{p/2} \exp\left[2i\pi \frac{f_0}{f} \varphi(x)\right] \exp\left(-2i\pi n \frac{x}{p}\right) dx. \tag{6}$$

Eq. (6) takes into account the wavelength dependence of the diffraction coefficients by the term f_0/f . This wavelength dependence occurs for phase gratings since the phase delay varies with the wavelength. Here, f_0 is the center frequency for which the grating was designed. Using Eq. (3) for the temporal domain it is sufficient to calculate with an average value using the approximation $f_0/f \approx 1$. However, using Eq. (5) for the calculation of the spectrum (in our case $f_0 \approx 372.5$ THz, $\Delta f \approx 37$ THz, $\lambda \approx 800$ nm, $\Delta \lambda \approx 79.5$ nm, respectively) we need not to give away the better accuracy in Eq. (6) and calculate the value of f_0/f .

3. Modeling the experimental setup

We model the propagation of a sequence of diffracted ultrashort pulses in the Talbot interferometer. For a stationary wave field behind a grating diffraction orders occur at discrete spatial frequencies, here expressed by the x -component of the wave vector as $k_x = 2\pi v = n(2\pi/p)$ (p : period

of the grating, n : diffraction order). In the n th order a shift of $n\lambda$ occurs (λ : wavelength).

The situation is more complex for ultra short pulses. It is visualized for the zeroth and first order in Fig. 4. In the zeroth order the temporal structure of the pulse remains unchanged behind grating G_1 (Fig. 4a). The directions of pulse front (envelope, $\Delta \vec{k}$) and wave front (carrier, \vec{k}) are in this case identical and both in the direction of the incident beam. For higher orders (Fig. 4b) pulse front and wave front are different. The pulse front is unchanged parallel to the grating, but wave fronts are tilted with an

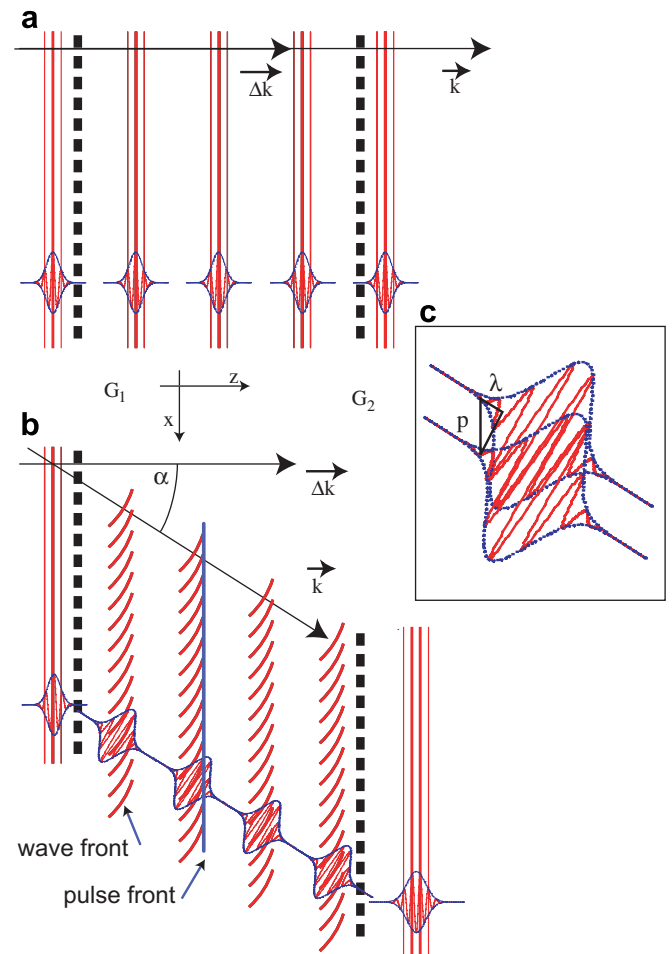


Fig. 4. Diffraction of a short pulse in a Talbot interferometer, (a) zeroth order, (b) first order, (c) pulse interference.

angle $\sin(\alpha_n) = n\lambda/p$. The above mentioned shift in the wave front of $n\lambda$ leads to the situation that a pulse can interfere with a shifted copy of itself. This is illustrated in Fig. 4c for the first order. The spatial shift in the n th order corresponds to a temporal delay of n/f_0 (f_0 temporal carrier frequency).

When the shift exceeds the pulse length no interference can occur any more. We write down the interference equation for two time pulses denoted by their temporal amplitudes $E(t)$ and shifted by t_s :

$$I(t) = \left\langle |E(t) + E(t + t_s)|^2 \right\rangle. \quad (7)$$

We consider a Gaussian pulse at the carrier frequency f_0 described as

$$E(t) = E_0 \exp\left(-\pi \left[\frac{t}{\Delta t}\right]^2\right) \cos(2\pi f_0 t). \quad (8)$$

With this Eq. (7) becomes (after normalization):

$$\begin{aligned} \frac{I(t)}{2I_0} &= \frac{\sqrt{2}}{E_0^2 \Delta t} \int_{-\infty}^{\infty} |(E(t_s) + E(t + t_s))|^2 dt_s \\ &\approx \exp\left[-\pi \left(\frac{t}{\sqrt{2}\Delta t}\right)^2\right] \cos(2\pi f_0 t) + 1. \end{aligned} \quad (9)$$

The first term on the right is the autocorrelation of the pulse and there occurs a unity offset. One can plot this function as a function of the time delay t_s . However, with the relations $t_s = s/c$ (s : spatial shift of two delayed pulses) and $s = p\sin(\alpha) = p\lambda\nu$ we can also show the intensity as a function of the spatial frequency ν (Fig. 5) since the following holds:

$$\frac{\nu}{\nu_1} = \nu p = t_s \cdot \frac{c}{\lambda} = t_s \cdot \text{const} \quad (10)$$

In Fig. 5, the integer values along the abscissa denote the diffraction orders. The local maxima of this curve appear exactly at integer values and indicate the pulse amplitude

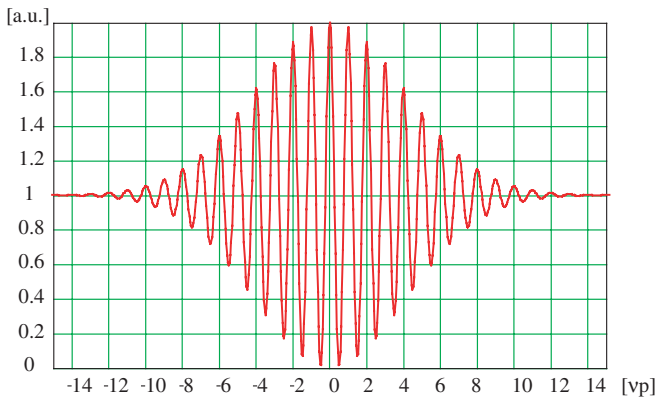


Fig. 5. Interference curve (abscissa with normalized diffraction orders $\nu/\nu_1 = \nu p \propto t$) for the used pulse to indicate orders with sufficient interference. The used pulse is Gaussian shaped with a duration of 27 fs and a carrier frequency of 372.5 THz (wavelength 800 nm). Until the order 10 the intensity has a significant ripple.

in the case of constructive interference of the pulse with a delayed copy of $n\lambda$, thus it represents the maximum intensity for a certain diffraction order, e.g., the zeroth order has full intensity with the level 2.0 while the third order has a significant decrease to the level 1.75. Beyond the 10th order there is no pronounced local maximum anymore, in the diffraction pattern this region exhibits a constant light intensity along the x -axis.

As a consequence, the pulse shearing admits significant diffraction orders only in a range with numbers smaller than $\Delta t f_0$ with Δt the temporal pulse width and f_0 the temporal frequency of the carrying light. With the conditions of the experiment this means $N < 27 \text{ fs} \cdot 372.5 \text{ THz} \approx 10$. To ensure a good contrast we shall even not exceed the third order.

By this consideration, we have determined the lower limit for the pulse duration. On the other hand, the pulse must not be too long in order to obtain temporal separation. The pulse duration Δt has to be shorter than the shortest time delay which is given as $\tau_1 = M\lambda/c$. For this restriction, there is a little margin available because in our experimental setup, we can adjust the separation of the two gratings to several self-imaging distances M . This margin is limited somewhat by walk-off effects, an obvious limitation is given by the temporal measurement range of the used autocorrelator. For our measurements we found and thus $\tau_1 \approx 12 \text{ fs}$ to supply workable results.

Summarizing the temporal restrictions of the experiment can be given by

$$\frac{M}{f_0} > \Delta t > \frac{N}{f_0}. \quad (11)$$

The higher limit is determined by the multiples M of the adjusted self-imaging distance and the lower limit is determined by the highest order that is yet capable to interfere.

Other considerations must deal with the design of the gratings. We use a phase grating pair that realizes even and odd orders with a period of $p = 6.21 \mu\text{m}$ and 1 mm thin substrates to avoid additional dispersion. The pulse broadening due to the dispersion of the glass substrate (HPFS-glass) was simulated to be 2 fs for pulses of 27 fs duration.

The essential device for the measurements is the autocorrelator (Fig. 6). A pulsed laser beam propagates through the Talbot interferometer, then enters the autocorrelator. Therein the beam is split up into two branches. One branch is variably delayed. Reunited the output beam passes a crystal with a quadratic transfer characteristic. At last, the modulated beam is directed to a photomultiplier. The generated electrical signal can be represented with the integral

$$I(t_d) = \frac{1}{T} \int_{-T/2}^{T/2} |(E(t) + E(t + t_d))|^2 dt. \quad (12)$$

If a single Gaussian pulse is supplied to the autocorrelator the normalized solution of the integral is shown to be

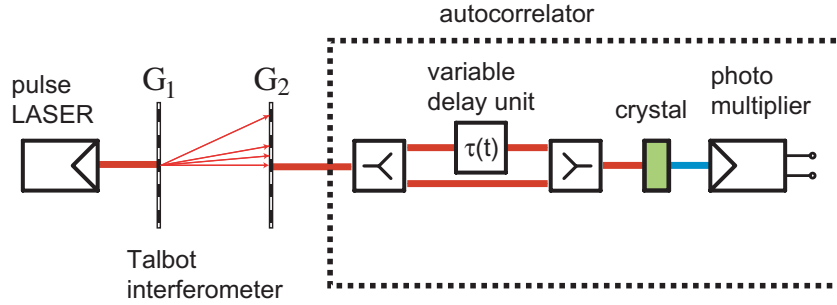


Fig. 6. Measurement of the temporal impulse response with an autocorrelator.

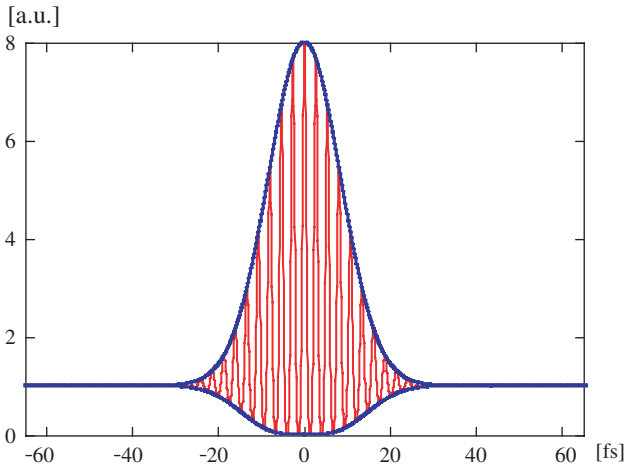


Fig. 7. Calculated output of the autocorrelator processing a single Gaussian pulse.

$$\frac{I(t_d)}{I(t_d \rightarrow \infty)} = \left\{ 1 + 2 \exp \left[-\pi \left(\frac{t_d}{\Delta t} \right)^2 \right] \left[1 + \frac{1}{2} \cos(\omega_0 2t_d) \right] + 4 \exp \left[-\pi \left(\frac{t_d}{\frac{2}{\sqrt{3}} \Delta t} \right)^2 \right] \cos(\omega_0 t_d) \right\} \quad (13)$$

by neglecting smaller terms. In Fig. 7 the curve and its envelope for this integral is illustrated. The typical shape of this curve can be characterized with the mean value unity, the bottom touching the temporal axis and a peak value of eight arbitrary units (a.u.).

If we transmit a Gaussian pulse through a Talbot interferometer, we expect a different pulse shape at the output. We use a discrete convolution to calculate the pulse shape according to Eq. (4) and obtain the result shown in Fig. 8. Obviously, the curve is symmetrical due to the operation implemented by the autocorrelator. It is thus sufficient to analyze one half of the curve. At the delays for second and third order a local maximum can be noticed. The pulse corresponding to the first order is hidden in the dominant central pulse for the zeroth order.

4. Experimental measurement of the impulse response

The measurements of the impulse response are performed with a pulsed laser source supplying pulses with a carrier wavelength of 800 nm. This corresponds to a temporal carrier frequency of 372.5 THz. The pulse duration is approximately 27 fs, the pulses have an almost Gaussian envelope. The pulse repetition rate is about 87 MHz. The Talbot interferometer consist of two phase gratings as described in Section 2. The period of each grating is 6.31 μm. To have not only odd diffraction orders the duty cycle was designed such that a significant second order occurs. The gratings were separated by a distance $\Delta z = 4 z_T = 24.7$ mm.

The pulse sequence detected by the autocorrelator is illustrated and compared with the calculated envelope in Fig. 9. The red curve¹ with carrier shows the measured

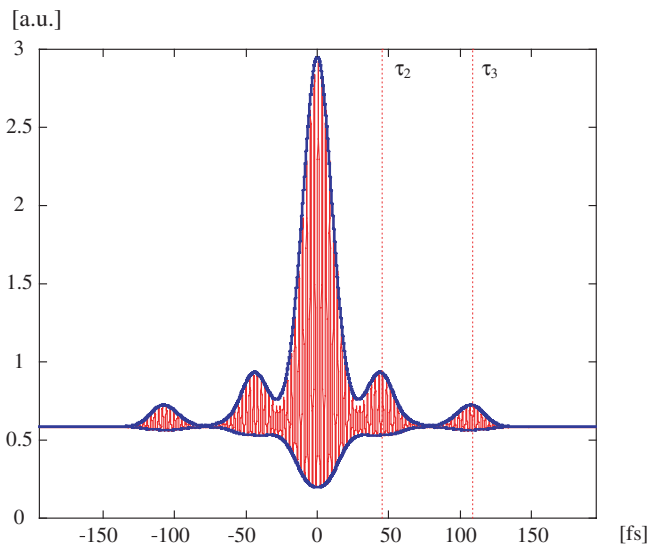


Fig. 8. Calculated output of the autocorrelator processing the output of the Talbot interferometer, horizontal axis in femtoseconds, vertical axis normalized units corresponding to Fig. 6.

¹ For interpretation of color in Fig. 9, the reader is referred to the web version of this article

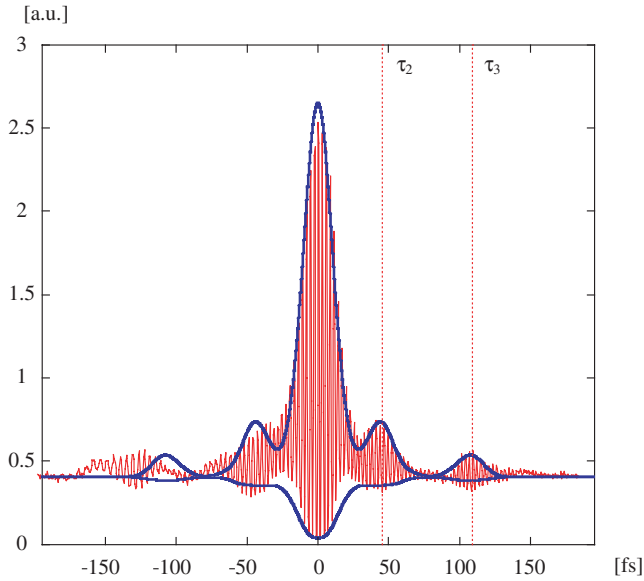


Fig. 9. Measured autocorrelation (with carrier) and modelled autocorrelation (envelope only). Horizontal axis in femtoseconds, vertical axis in normalized units.

autocorrelation as it is recorded by the measurement device. The blue curve is the calculated envelope according to the explanations in the previous section. The linear measurement range was exceeded by both wingtips of the autocorrelator's pulse pattern. To have at least one wing undistorted the linear range was shifted completely to one wing, the left wing thus exhibits strong temporal nonlinearities. However, in the right half of this curve we can exactly recognize the temporal position of the output pulses.

For the grating separation given above, we expect the first output pulse from the Talbot interferometer after a delay of approximately 12 fs. Since the width of the central peak is larger than this value, the first pulse disappears in

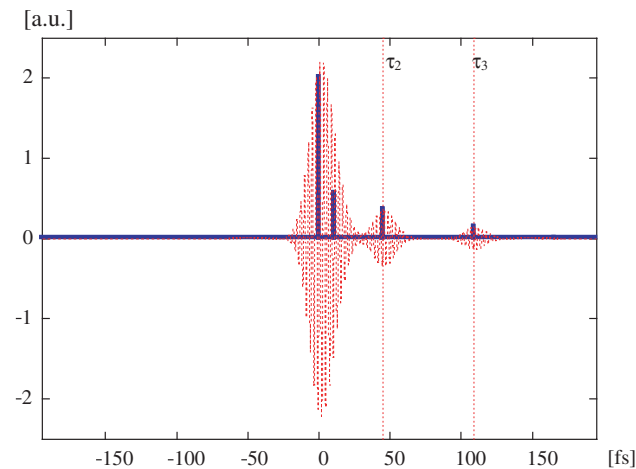


Fig. 10. Modeled response of the Talbot interferometer (Dirac pulses) and its convolution with the input Gaussian pulse. Horizontal axis in femtoseconds, vertical axis in normalized units.

the central peak. However, separated peaks for the second and third pulse occur at 48 and 108 fs, respectively, and can be identified well. The measured values for the time delays and the amplitudes of the peaks match almost perfectly the calculated curve. As a result the measurement fits nearly perfectly the calculated curve represented in Fig. 9 by its envelope. By deconvolution, we can derive the blue peaks shown in Fig. 10 which mark the delays of the different output pulses from the Talbot interferometer.

5. Measurement of the power spectrum transmission

After measuring the impulse response in the time domain, we now measure the corresponding power spectrum characteristics in the spectral domain. As pointed out earlier, we cannot measure the transfer function of the Talbot interferometer directly, but only the optical power spectrum. The temporal frequency response was already given with Eq. (5), the following extended version shows the frequency dependencies in detail:

$$H(f) = \sum_{n=0}^N a_n(f) \exp\left(2i\pi \frac{f}{f_0} \frac{Mz_T p f_0^2}{c\sqrt{p^2 f_0^2 - n^2 c^2}}\right). \quad (14)$$

The coefficients $a_n(f)$ have a frequency dependency as specified in Eq. (6) for $b_n(f)$ and are calculated as their squared absolute value. In the exponent Mz_T (=multiple of the Talbot distance) occurs as well as the grating period p . For the used wavelength, $\lambda_0 = 800$ nm, the carrier frequency equals $f_0 = c/\lambda_0 \cong 372.5$ THz. The output power spectrum can be expressed as

$$|S_{\text{out}}(f)|^2 = |S_{\text{in}}(f)|^2 |H(f)|^2. \quad (15)$$

The calculated curve for $|H(f)|^2$ is presented in Fig. 11 (small red line).

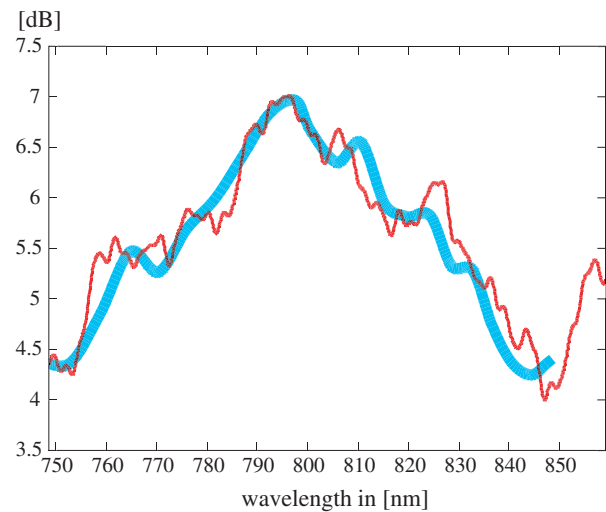


Fig. 11. Power spectrum of the investigated Talbot interferometer. The red (small) continuous curve is calculated, the cyan (bold) curve is measured. (For interpretation of the references in colour in this figure legend, the reader is referred to the web version of this article.)

For the measurements, an adjustable laser source with a tuning range from 750 to 850 nm and a high resolution spectrometer were used. The output amplitudes are referred to the input amplitudes, thus the input signal can be regarded being constant over the frequency range. The resolution was approximately 0.1 nm. For each measurement step the wavelength was increased and remained in force. The plot of the referenced intensities over the temporal frequency then directly results in the power spectrum. The measured curve (bold cyan) for the power spectrum of the Talbot interferometer is compared to the calculated curve (small red line) in Fig. 11. The measured curve progresses more smoothly. The cause for this observation is a low pass characteristic of the measurement equipment. However, given the difficulties of the measurement, one can conclude that calculated and measured curve are in good agreement.

6. Conclusions

We demonstrated in good agreement with preceding explanations the temporal impulse response of a Talbot interferometer. The expected response was verified by

experiments using ultra short pulses in the femtosecond range. Even though the presented formulas utilize some approximations, their accuracy is quite good. Further, the presented time delays are appropriate for calculations of the power spectrum. The measurement of the power spectrum for the Talbot interferometer and the relevant calculations confirm good consistency of the results.

With this confirmation of preceding theoretical work [3], other types of interferometers can be investigated now, e.g., the Montgomery interferometer with linearly increasing time delays [6] as the more general extension of the Talbot interferometer. The good results obtained here to lead to applications in the context of short pulses and code division multiplex techniques in which the interferometers can serve as decoder and encoder for pulse sequences.

References

- [1] H.F. Talbot, *Phil. Mag.* 9 (1836) 401.
- [2] A.W. Lohmann, D.E. Silva, *Opt. Commun.* 2 (1971) 413.
- [3] J. Jahns, E. El Joudi, D. Hagedorn, S. Kinne, *Optik* 112 (2001) 295.
- [4] J. Azaña, M.A. Muriel, *Appl. Opt.* 38 (1999) 6700.
- [5] J. Jahns, A.W. Lohmann, *Appl. Opt.* 43 (2004) 4339.
- [6] G. Mínguez-Vega, J. Jahns, *Opt. Commun.* 236 (2004) 45.